Marine Chemistry 274 (2026) 104601

Contents lists available at ScienceDirect

Marine Chemistry

journal homepage: www.elsevier.com/locate/marchem

Phosphorus speciation and C:N:P stoichiometry in particles in the East Sea (Japan Sea), Northwest Pacific

Chihyun Oh, Taehee Na, Jeomshik Hwang *

School of Earth and Environmental Sciences/Research Institute of Oceanography, Seoul National University, Seoul, South Korea

ARTICLE INFO

Keywords:
Phosphorus speciation
Sediment traps
C:N:P stoichiometry
Sediment resuspension

ABSTRACT

Particulate phosphorus (P) can exist in several species, particularly in marginal seas, where sediment resuspension can affect particle fluxes. The effect of P speciation on the C:N:P stoichiometry of particulate organic matter is poorly constrained. We investigated the C:N:P stoichiometry in the East Sea (Japan Sea), which is a marginal sea in the Northwest Pacific, by analyzing sinking particles collected at water depths of 500, 1000, and 2250 m (i.e., 50 m above the seafloor), along with suspended particles in the surface waters and the underlying sediments. We measured particulate organic carbon (POC), particulate nitrogen (PN), and particulate P. The P was separated into total P (TP), organic P (OP), inorganic P (IP), non-apatite inorganic P (NAIP), and apatite P (AP) following the Standards, Measurements, and Testing (SMT) protocol of the European Commission. In addition, Al, Si, and Ca were analyzed to estimate the contents of lithogenic material, opal, and $CaCO_3$ in the sinking particles. The POC:PN ratio increased from 8.2 at 500 m water depth to 8.9 in the surface sediment, whereas the POC:TP and PN:TP ratios decreased from 229 and 28 at 500 m to 68 and 7.6 in the surface sediment, respectively. The IP flux exhibited a strong positive correlation with the Al flux ($R^2 = 0.92$), which is a proxy for material derived by sediment resuspension. After correction based on the content of Al, to eliminate the contribution from sediment resuspension, nearly all of the IP was accounted for by the resuspension-derived fraction, implying that sediment resuspension could be the dominant source of IP in sinking particles in a marginal sea environment. The mean biogenic (i.e., resuspension-corrected) C:N:P ratios were 238:36:1 in suspended particles in the surface water, 444:56:1, 359:45:1, 329:37:1 in sinking particles at water depths of 500, 1000, and 2250 m, respectively, and 109:12:1 in the surface sediment. The biogenic C:N:P stoichiometry suggests that surface IP is labile and subject to rapid recycling in the upper 500 m of the sea. We suggest that C:TP is an appropriate measure of the stoichiometry of biogenic particles in the upper layer, whereas C:OP is more appropriate for sinking particles affected by resuspension in the deeper interior of the sea.

1. Introduction

The C:N:P ratio in plankton samples is generally 106:16:1 (Redfield et al., 1963). However, observational and modeling studies have reported deviations from this ratio for suspended and sinking particles (Arrigo et al., 1999; Faul et al., 2005; Koeve and Kähler, 2010; Kwon et al., 2022b; Martiny et al., 2013, 2014; Matsumoto et al., 2020; Teng et al., 2014). Martiny et al. (2013) compiled global particulate C:N:P data from >700 stations and reported that the C:N ratios showed little variation whereas the C:P and N:P ratios exhibited substantial variability. The variations in C:P and N:P ratios have been attributed to factors such as nutrient availability (Galbraith and Martiny, 2015), growth rate (Karl et al., 2001), upwelling intensity (Benitez-Nelson et al., 2007; Mills and Arrigo, 2010), phytoplankton class, temperature (Garcia et al., 2018), plankton community structure (Karl et al., 2001; Liefer et al., 2024; Lomas et al., 2022; Tanioka and Matsumoto, 2020), and light availability (Laws and Bannister, 1980; Sakshaug and Holm-Hansen, 1977).

The variability in C:P and N:P ratios has important implications for P-based models of carbon cycling. For example, the variability in the C:N:P ratio introduces large uncertainties in estimates of primary production and organic matter export production (Kwon et al., 2022a; Teng et al., 2014). Teng et al. (2014) suggested that assuming a fixed C:P ratio may result in large errors of up to three- to four-fold when estimating the global organic matter export production. In this context, using accurate C:N:P ratios in models is essential. However, such high temporal

* Corresponding author.
E-mail address: jeomshik@snu.ac.kr (J. Hwang).

https://doi.org/10.1016/j.marchem.2025.104601
Received 2 July 2025; Received in revised form 12 December 2025; Accepted 17 December 2025
Available online 18 December 2025

resolution data for primary producers do not exist. Sediment trap data for particulate C:N:P stoichiometry as alternatives are limited. Previous studies at two long-term monitoring stations, the Hawaiian Ocean Time-series (HOT) and Bermuda Atlantic Time-series Study (BATS), yielded conflicting results in the changes in C:N:P stoichiometry in the upper water layer (Teng et al., 2014).

In the ocean interior, the transport of P by sinking particles is a major pathway for the removal of P from the surface layer and provides a link between the carbon and nutrient cycles (Paytan and McLaughlin, 2007; Zhao et al., 2024). Phosphorus cycling in the water column can be better understood when P species are considered in addition to total P. Faul et al. (2005) suggested that preferential removal of labile P occurs at relatively shallow water depths (< 300 m), and that measurements restricted to the acid-insoluble P fraction would result in underestimation of the biologically derived P. Benitez-Nelson et al. (2007) suggested that organic P is rapidly remineralized in oxic surface waters, whereas inorganic P is released under anoxic conditions through the dissolution of metal oxides. Lyons et al. (2011) reported strong correlations (R^2 > 0.85) between the lithogenic flux and fluxes of authigenic P and detrital P, implying that a significant fraction of inorganic P is terrestrially derived. This is important in studies of P cycling in marginal seas, where sediment resuspension is prevalent and can be a significant source of particulate P in deep waters. Few studies have attempted to quantify the contribution of sediment resuspension to particulate P fluxes and to understand its effect on particulate C:N:P stoichiometry.

The East Sea (also known as the Japan Sea) is a semi-enclosed basin surrounded by Korea, Japan, and Russia. Seawater exchange with the North Pacific occurs through straits shallower than 200 m (Fig. 1). Due to rapid ventilation, deep waters in the basin have relatively high concentrations of dissolved oxygen (>200 μmol kg^{-1}; Kim and Kim, 1996). The Ulleung Basin (UB; maximum depth = 2300 m), located in the southwestern East Sea, has the highest primary production in the East Sea (Kwak et al., 2013). There are no large rivers that flow directly into the basin. Sediment resuspension is prevalent on the southern slope and in the basin (Kim et al., 2020; Lee et al., 2019; Seo et al., 2023). In the UB, the C:N:P ratio for surface suspended particles is 107:11:1 (Chen et al., 1996). Here we present the first report of the particulate C:N:P stoichiometry in the UB. We attempted to investigate the changes in C:N:P stoichiometry along the biological pump (i.e., from suspended particles in the surface waters to sinking particles collected at three depths on a mooring line, as well as in the underlying sediment). To further understand the causes of the variations in the C:N:P stoichiometry, we fractionated the particulate P into five species. In addition, we attempted to evaluate the effect of sediment resuspension on the P fluxes and C:N:P stoichiometry.

2. Methods

2.1. Sample collection

To collect the sinking particle samples, sediment traps (SMD6000–26 s; NiGK, Japan) were moored at station EC1 (37°19′N, 131°25′E; bottom depth = 2300 m) in the UB. The traps were placed at depths of 500, 1000, and 2250 m (i.e., 50 m above the seafloor) from 13 November 2020 to 8 December 2021. The preservation solution consisted of seawater collected on-site that was fortified with NaCl (5 g/L) and $HgCl_2$ (3 g/L). The samples were collected at 15-d intervals. Samples were only available for the period from 13 November 2020 to 11 April 2021 due to a trap malfunction after May 2021. Surface sediment samples were collected in the central part of the basin using a box corer onboard the R/V *Onnuri* on 5 November 2020 (KU10) and 21 November 2023 (DB). Waters for the suspended particle samples were collected using Niskin bottles during the research cruises of the R/V *Onnuri* in May and November 2023. The collected seawater samples were filtered through pre-combusted GF/F filters onboard the vessel, and the filters were stored frozen at −80 °C before being transferred to a − 20 °C freezer in the laboratory.

2.2. Sample analysis

All the glassware used in the experiments was pre-cleaned with 10 % HCl and Milli-Q water, and combusted at 450 °C for 4 h. Plasticware was cleaned using phosphate-free detergent (Extran), followed by 10 % HCl and rinsing with distilled water.

2.2.1. Sediment trap sample preparation and flux calculations

The sinking particle samples were filtered through a 1 mm nylon mesh to remove swimmers, and then divided into 10 equal aliquots using a wet sample divider (WSD-10; McLane, USA). One aliquot was filtered through a PCTE membrane filter (1.0 μm; Whatman), rinsed with Milli-Q water, freeze-dried, and weighed for the total mass flux (TMF). The TMF was calculated as TMF = 10 × dry mass of one aliquot ÷ sediment trap opening area ÷ sampling period. The flux of each component was then calculated by multiplying the TMF and content of

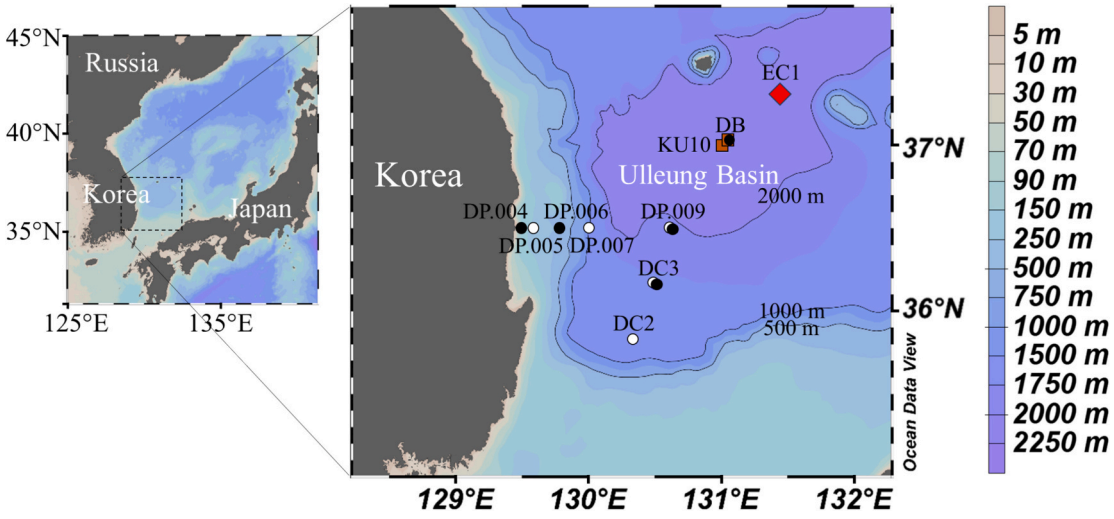

Fig. 1. Map of the study area showing the sampling sites. Sinking particle samples were collected at EC1 (◆). Suspended particles were collected at two different times (○ = May 2023; ● = November 2023) at stations DP, DC, and DB. Surface sediments (■) were obtained at stations KU10 and DB in the central part of the basin.

the component.

2.2.2. Particulate P species

Analysis of the P species followed the Standards, Measurements, and Testing (SMT) protocol developed by the European Commission (Fig. 2). This protocol is a modified version of the method proposed by Williams et al. (1976). Compared with other approaches, this method has good interlaboratory relative standard deviations that are typically <10 % (Ruban et al., 1999). In addition, a certified reference material (CRM), BCR-684, is available for quality assurance (Ruban et al., 1999, 2001). The SMT protocol enables the quantification of five P fractions: total P (TP), organic P (OP), inorganic P (IP), non-apatite inorganic P (NAIP), and apatite P (AP). The NAIP fraction is associated with Al-, Fe-, and Mn-bound P, and the AP fraction is associated with Ca-bound P. The NAIP fraction may also contain loosely adsorbed P fraction because this fraction was not separately removed using milder solvents (Ruttenberg, 1992). The SMT protocol can determine TP, which is commonly used to evaluate bulk C:N:P ratios, and distinguish between OP and IP to assess the forms and sources of particulate P. Furthermore, IP was separated into NAIP and AP to characterize its specific mineral associations.

Each particulate sample was divided into three aliquots. The first aliquot was combusted at 450 °C for 3 h, stirred with 3.5 N HCl for 16 h, and then the supernatant was processed to obtain TP. The second aliquot was stirred with 1 N HCl for 16 h, and the supernatant was processed to obtain IP. The remaining particulate sample was rinsed with Milli-Q water, combusted at 450 °C for 3 h, and then stirred again with 1 N HCl for 16 h to obtain OP. The third aliquot was extracted using 1 N NaOH with 16 h of magnetic stirring, and the supernatant was processed to obtain NAIP. The remaining particulate sample was rinsed with 1 M NaCl and then stirred with 1 N HCl for 16 h. The supernatant was processed to obtain the AP. According to the extraction scheme, TP should contain the OP and IP, and IP should contain the NAIP and AP (TP ≈ OP + IP; IP ≈ NAIP + AP). The samples were diluted 10 or 20 times prior to analysis. Phosphate analysis was conducted by UV–Vis spectrophotometry following the method of Murphy and Riley (1962). Calibration curves were prepared using a KH_2PO_4 standard, and each experiment was validated using a CRM (BCR-684; European Commission). The average recoveries of TP, IP, OP, NAIP, and AP were 92 % ± 3 % (n = 18), 96 % ± 3 % (n = 23), 99 % ± 5 % (n = 13), 104 % ± 5 % (n = 8), and 85 % ± 3 % (n = 8), respectively. For the suspended particle samples, only the OP and IP were measured due to the limited amount of sample, and their sum was considered to be TP. No procedural blank was detected.

2.2.3. Organic carbon, total nitrogen, Al, Ca, and Si

The PN was measured using an elemental analyzer (2400 Series II CHNS/O; PerkinElmer). For POC analysis, samples were weighed into Ag capsules, fumed with concentrated HCl in a desiccator for 20 h, and then left on a 45 °C hotplate for 4 h before being placed in Sn capsules for analysis. For the suspended particle samples, 25 % of each filter was used for POC and PN measurements. Surface sediment and suspended particle samples were also treated with HCl fumigation prior to determining POC and PN contents.

The Al, Ca, and Si contents were measured at the Korea Basic Science Institute (KBSI), Daejeon, South Korea. Samples were digested in a mixed acid solution of HNO_3, $HClO_4$, and HF on a hotplate at 170 °C. Aluminum, Ca, and Si were analyzed by inductively coupled plasma–atomic emission spectrometry (ICP–AES; Optima 8300; PerkinElmer). The lithogenic content was estimated as follows: lithogenic content = 12.15 × Al content (Honjo et al., 1995; Taylor and McLennan, 1985). Biogenic Ca was estimated as follows: biogenic Ca = total Ca − lithogenic Ca, where lithogenic Ca = 0.5 × Al content (Honjo et al., 1995). The $CaCO_3$ content was then obtained as follows: 2.5 × biogenic Ca. Biogenic Si was calculated as follows: biogenic Si = total Si − lithogenic Si, where lithogenic Si = 3.5 × Al content (Honjo et al., 1995). Opal content was calculated as follows: opal = 2.4 × biogenic Si (Mortlock and Froelich, 1989). The particulate organic matter (POM) content was calculated as follows: POM = 1.88 × POC (Lam et al., 2011).

2.3. Satellite-based net primary production and sea surface temperature data

Net primary production (NPP) data were obtained from the Ocean Productivity project, which provides 8-d composites generated using the vertically generalized production model (http://sites.science.oregonstate.edu/ocean.productivity; Behrenfeld and Falkowski, 1997). We used data from the 1° × 1° grid cell that includes the study area. Sea surface temperature (SST) data were obtained from the NOAA Optimum Interpolation SST dataset, which combines satellite observations and in situ measurements to produce SST fields at 8-d and monthly resolutions (https://downloads.psl.noaa.gov/Datasets/noaa.oisst.v2.highres; Reynolds et al., 2002). We used data from the 1° × 1° grid cell that includes the study area.

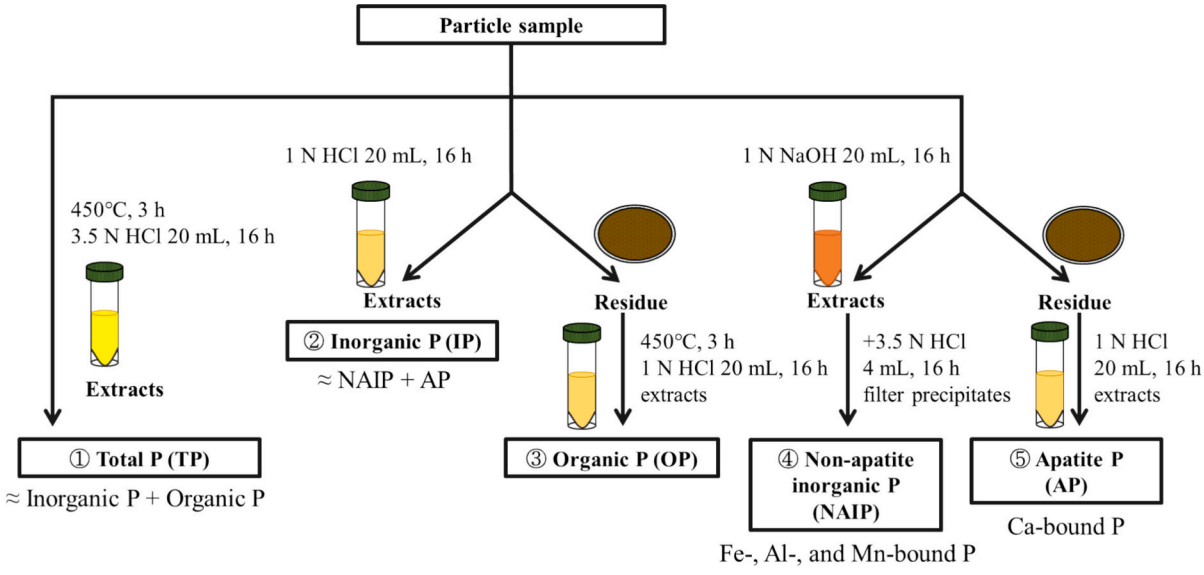

Fig. 2. The P species extraction procedure based on the Standards, Measurements, and Testing (SMT) protocol of the European Commission (Ruban et al., 1999).

2.4. Estimation of resuspension-derived and primary-production-derived fluxes

To estimate the fraction of the sinking particle flux derived by sediment resuspension, we assumed that all Al in the sinking particles originated from sediment resuspension (Kim et al., 2017, 2020; Seo et al., 2023). We also assumed that the elemental molar ratios of the surface sediment remained unchanged during resuspension. We used literature data for Al contents (4.8 wt%) for the surface sediment in the central UB (Cha et al., 2007). For example, the resuspension-derived IP content was calculated as follows:

$$\text{resuspension} - \text{derived IP} = (\text{IP/Al in sediment}) \times (\text{Al content in sinking particles}),$$

where "IP/Al in sediment" was measured to be 0.0109 mol mol^{-1}. Similarly, the resuspension-derived contents of POC, PN, and OP were calculated as follows:

$$\text{resuspension} - \text{derived X} = (\text{X/Al in sediment}) \times (\text{Al in sinking particles}),$$

where X = POC, PN, and OP.

Primary-production-derived fluxes of C, N, and P were reconstructed by subtracting the resuspension-derived fraction from each elemental flux. C:N:P ratios were reconstructed for the sinking particles using primary-production-derived POC, PN, and OP fluxes. In the case of suspended particles in the surface waters, the measured C:N:TP ratios were used. To estimate the C:N:P ratio of the non-lithogenic fraction in the surface sediment, lithogenic inputs were subtracted using the N:Al (0.00593) and P:Al (0.00699) ratios of the upper crust (Rudnick and Gao, 2003), along with the Al content (Cha et al., 2007) in the sediment. While regional deviations may exist, this approach provides a first-order approximation of the primary-production-derived C:N:P stoichiometry.

3. Results

3.1. Satellite-based net primary production and sea surface temperature

Satellite-based 16-d average NPP during the period of sediment trap sampling ranged from 367 to 1290 mg C m^{-2} d^{-1} (Fig. 3). NPP was high in November (1167 mg C m^{-2} d^{-1}), decreased abruptly in early December (460 mg C m^{-2} d^{-1}), and reached a minimum of 367 mg C m^{-2} d^{-1}. It remained relatively stable thereafter, increased slightly in February, and then increased abruptly in March, reaching 1031 mg C m^{-2} d^{-1} in mid-March and peaking at 1290 mg C m^{-2} d^{-1} in early April. The daily SST was 19.0 °C in mid-November, decreased gradually to a minimum of 10.8 °C in March, and then increased again to 14.2 °C in early April (Fig. 3).

3.2. Contents and fluxes of POC, PN, and P species in the sinking particles

The average TMF was 401, 443, and 559 mg m^{-2} d^{-1} at water depths of 500, 1000, and 2250 m, respectively (Table 1). The TMF at 2250 m water depth was the highest of all water depths during most sampling periods (Fig. 3; Table S1). Temporally, the TMF at all depths peaked in November, followed by a substantial decrease in December (Fig. 3). The TMF then increased until April. At 2250 m, the TMF peaked again in April, reaching a level comparable to that in November, whereas the TMF at 500 and 1000 m in April was ~40 % and ~ 50 % of the November flux, respectively. This seasonal pattern is broadly consistent with that of the NPP. However, the high NPP values in March and April are not reflected proportionally in the TMF at 500 m (Fig. 3).

The average POC, PN, and TP contents of the sinking particles decrease with increasing water depth (Fig. 3; Table 1), with the relative decrease being smallest for TP. Temporally, the POC and PN contents at 500 m peaked in December, decreased until February, and then increased towards April (Fig. 3). A similar trend was observed at 1000 m. In contrast, at 2250 m, both the POC and PN contents were relatively uniform. The TP contents showed a different temporal trend as compared with POC and PN. The highest values were observed in November, followed by a general decrease until March (Fig. 3).

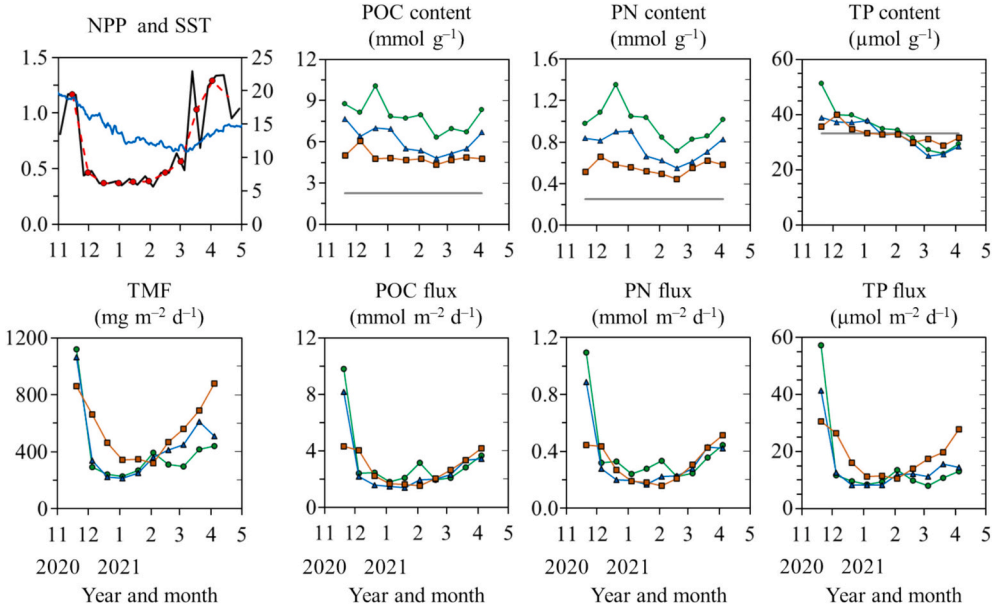

Fig. 3. Temporal variations in net primary production (NPP), sea surface temperature (SST), and POC, PN, and TP contents (upper row) at the sediment trap mooring site. Horizontal lines indicate the average values in the surface sediment for each parameter. The lower row shows the total mass flux (TMF) and POC, PN, and TP fluxes. Symbols denote depths of 500 m (●), 1000 m (▲), and 2250 m (■). NPP (g C m^{-2} d^{-1}, left *y*-axis) is shown as 8-d (black line) and 16-d (red dots) averages from 31 October 2020 to 14 April 2021. SST (°C, right y-axis) is shown as a blue line. The 16-d average NPP (red dots) approximately matches the sediment trap sampling intervals. (For interpretation of the references to colour in this figure legend, the reader is referred to the web version of this article.)

Table 1
Average ± standard deviation of the contents and fluxes of the POC, PN, P species, lithogenic material, opal, and $CaCO_3$ in the suspended particles in surface waters, sinking particles at 500, 1000, and 2250 m depths, and surface sediments. Fluxes are only presented for sinking particles, and the total mass flux at the three depths is also shown. Also proportions of OP and IP relative to TP, and proportions of NAIP and AP relative to IP are presented.

		Unit	Surface suspended particles	Sinking particles			Surface sediment (n = 2)
				500 m	1000 m	2250 m	
Total mass	Flux	mg d^{-1} m^{-2}		401 ± 262	443 ± 252	559 ± 207	
POC	Content	%	26 ± 6	9.5 ± 1.3	7.3 ± 1.2	5.8 ± 0.5	2.7
	Flux	mmol d^{-1} m^{-2}		3.2 ± 2.4	2.8 ± 2.0	2.7 ± 1.1	
PN	Content	%	4.7 ± 1.3	1.4 ± 0.2	1.0 ± 0.2	0.8 ± 0.1	0.4
	Flux	mmol d^{-1} m^{-2}		0.39 ± 0.26	0.33 ± 0.22	0.31 ± 0.13	
TP	Content	μmol g^{-1}	84 ± 17	35.1 ± 7.5	32.5 ± 5.2	33.0 ± 3.2	33.2
	Flux	μmol d^{-1} m^{-2}		15.2 ± 14.9	14.4 ± 9.8	18.5 ± 7.4	
OP	Content	μmol g^{-1}	49 ± 17	20.7 ± 1.4	19.5 ± 2.3	18.7 ± 2.3	11.4
	Flux	μmol d^{-1} m^{-2}		8.6 ± 6.6	9.0 ± 6.5	10.6 ± 4.5	
IP	Content	μmol g^{-1}	34 ± 15	10.1 ± 5.3	9.6 ± 3.4	12.2 ± 1.8	19.4
	Flux	μmol d^{-1} m^{-2}		5.0 ± 7.4	4.0 ± 3.0	6.7 ± 2.5	
NAIP	Content	μmol g^{-1}		8.5 ± 4.3	7.8 ± 2.3	9.3 ± 1.1	15.3
	Flux	μmol d^{-1} m^{-2}		4.2 ± 6.3	3.3 ± 2.2	5.2 ± 2.0	
AP	Content	μmol g^{-1}		3.7 ± 1.5	4.0 ± 1.2	4.9 ± 1.1	5.9
	Flux	μmol d^{-1} m^{-2}		1.5 ± 1.2	1.7 ± 0.9	2.6 ± 0.9	
Lithogenic material	Content	%		25 ± 9	27 ± 9	42 ± 8	
	Flux	mg d^{-1} m^{-2}		107 ± 108	121 ± 96	234 ± 101	
Opal	Content	%		49 ± 13	45 ± 13	42 ± 8	
	Flux	mg d^{-1} m^{-2}		190 ± 95	205 ± 123	222 ± 96	
$CaCO_3$	Content	%		8.8 ± 2.4	8.4 ± 2.0	6.1 ± 1.1	
	Flux	mg d^{-1} m^{-2}		35 ± 26	36 ± 21	34 ± 16	
OP/TP	Proportion	%	58 ± 14	61 ± 11	61 ± 10	57 ± 6	35 ± 5
IP/TP	Proportion	%	42 ± 14	27 ± 8	29 ± 7	37 ± 5	58 ± 2
NAIP/IP	Proportion	%		88 ± 20	85 ± 16	77 ± 6	79 ± 5
AP/IP	Proportion	%		38 ± 9	44 ± 6	40 ± 7	31 ± 4

The POC and PN fluxes show no clear changes with differences with depth (Fig. 3; Table 1), except for the first sampling period in November, when the fluxes were particularly high. Temporally, the POC and PN fluxes decreased significantly after peaking in November, and then increased again until April (Fig. 3). However, the fluxes at 500 and 1000 m in April were only ~40 % of those in November.

The OP was the dominant P species, accounting for 47 %–81 % (average = 60 %) of the TP. The average OP contents decreased slightly with water depth (Table 1). The average IP contents were generally higher at 2250 m (Fig. 4), with NAIP representing >70 % of the IP at all depths (Table S1). The AP was the least abundant P species (Fig. 4). The contents of NAIP and AP tended to be higher at 2250 m than at shallower water depths (Table 1). Temporally, the OP contents exhibited little variability (Fig. 4). The IP content at 500 m was highest in November and decreased thereafter (Fig. 4). At 1000 m, the IP contents remained relatively stable until February and then decreased until early April, whereas at 2250 m, temporal variability was minimal. The NAIP contents exhibited a similar trend to that of the IP. The AP content showed a slightly decreasing trend, but within a narrow range (Fig. 4).

Except for the first samples, the TP, OP, IP, NAIP, and AP fluxes showed little difference between 500 and 1000 m, whereas those at 2250 m were generally higher (Fig. 4; Table 1). The TP and OP fluxes had similar temporal variations at all water depths, resembling that of POC, with a peak in November, a decrease until January, and an increase from then towards April (Figs. 3 and 4). The IP, NAIP, and AP fluxes at 500 and 1000 m remained relatively stable from January to April. However, at 2250 m, the IP and NAIP fluxes increased from January to April (Fig. 4).

3.3. *Contents of POC, PN, and P species in suspended particles in surface waters and surface sediments*

At two sites near the sediment trap mooring, the surface sediments contained average POC of 2.7 wt%, PN of 0.4 wt%, and TP of 33.2 μmol g^{-1} (Fig. 3; Table 1). The average OP and IP contents were 11.7 and 19.4 μmol g^{-1}, respectively. The OP and IP represent ~35 % and ~ 60 % of the TP, respectively (Table 1). The average NAIP and AP contents were 15.3 and 5.9 μmol g^{-1}, respectively. The NAIP and AP represent ~80 % and ~ 30 % of the IP, respectively (Table 1).

In the suspended particles in the surface waters, the POC, PN, and TP concentrations were considerably higher in May than November (Table S2). The average POC concentrations were 28 μmol L^{-1} in May and 7.2 μmol L^{-1} in November, while the PN concentrations were 4.3 and 1.1 μmol L^{-1}, respectively. The P species were also higher in May. The TP concentrations averaged 0.154 μmol L^{-1} in May and 0.027 μmol L^{-1} in November, the OP concentrations averaged 0.076 and 0.015 μmol L^{-1}, and the IP concentrations averaged 0.078 and 0.012 μmol L^{-1}, respectively (Table S2).

The weight of suspended particles was only determined for the samples collected during November. As such, the POC, PN, and P contents, defined on a per mass basis, were only available for the November samples (Table S2). The average POC content was 26 wt% ($n = 5$), which is almost three times higher than the 9.5 wt% in the sinking particles at 500 m water depth (Table 1). The average PN content was 4.7 wt%, which is more than three times higher than the 1.4 wt% for sinking particles at 500 m. The average OP content was 49 μmol g^{-1}, as compared with the value of 20.7 μmol g^{-1} at 500 m. The average IP content was 34 μmol g^{-1}, higher than the value of 10.1 μmol g^{-1} at 500 m (Table 1).

At all depths, the POC flux correlated well with the TMF ($R^2 = 0.67$; $p < 0.001$) and the PN flux ($R^2 = 0.95$; $p < 0.001$), and also with the TP ($R^2 = 0.63$; $p < 0.001$) and OP ($R^2 = 0.78$; $p < 0.001$) fluxes (Fig. S1). The correlation between the POC and IP fluxes was weak when all depths were considered ($R^2 = 0.16$; $p < 0.05$), whereas the correlation between the TMF and IP flux was moderate ($R^2 = 0.52$; $p < 0.001$). When only considering a water depth of 2250 m, the IP flux was correlated strongly with both the TMF ($R^2 = 0.89$, $p < 0.001$) and POC flux ($R^2 = 0.85$; $p < 0.001$). The IP flux was also strongly correlated with the NAIP ($R^2 = 0.92$; $p < 0.001$) and AP ($R^2 = 0.91$; $p < 0.001$) fluxes (Fig. S1).

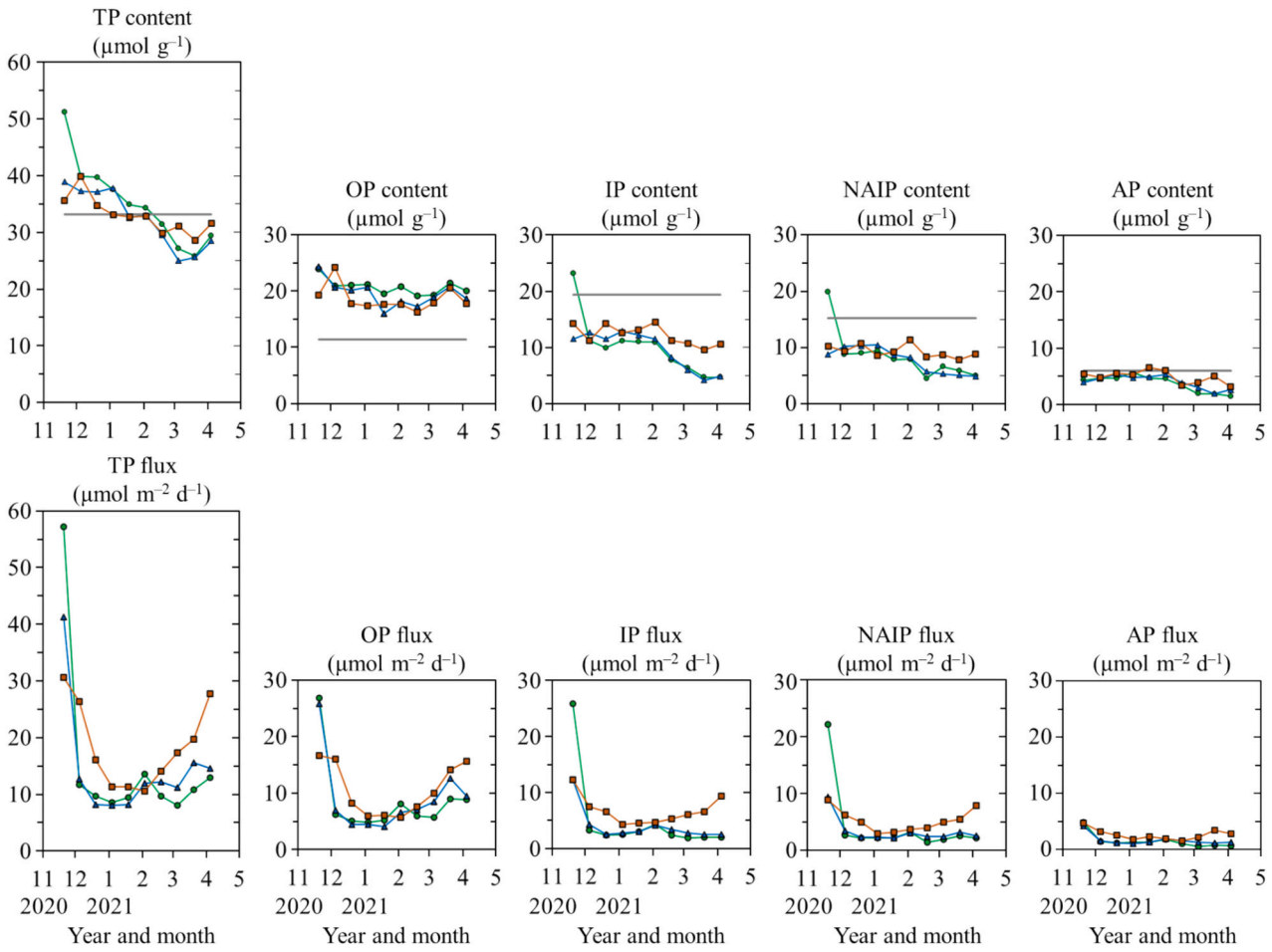

Fig. 4. Temporal variations in the contents (upper row) and fluxes (lower row) of TP, OP, IP, NAIP, and AP at water depths of 500 m (●), 1000 m (▲), and 2250 m (■). All P species are plotted on the same *y*-axis scale. Horizontal lines indicate the average values in the surface sediment for each parameter.

3.4. Ratios of C, N, and P

The mean C:N ratio of the suspended particles in the surface waters was 6.7 (Table S2), similar to the Redfield ratio. In the sinking particles, the mean ratios were 8.2, 8.2, and 8.9 at 500, 1000, and 2250 m, respectively, which are all higher than the Redfield ratio (Table S1; Fig. S2). In the surface sediment, the ratio was 8.9, similar to that at 2250 m.

The C:OP ratio in the suspended particles was 424 (Table S2) and decreased with depth, with values of 380, 312, and 261 for sinking particles at 500, 1000, and 2250 m, respectively. The ratio in the surface sediment was even lower at 195 (Fig. S2). The N:OP ratio showed a similar trend, with values of 64 in the suspended particles; 47, 38, and

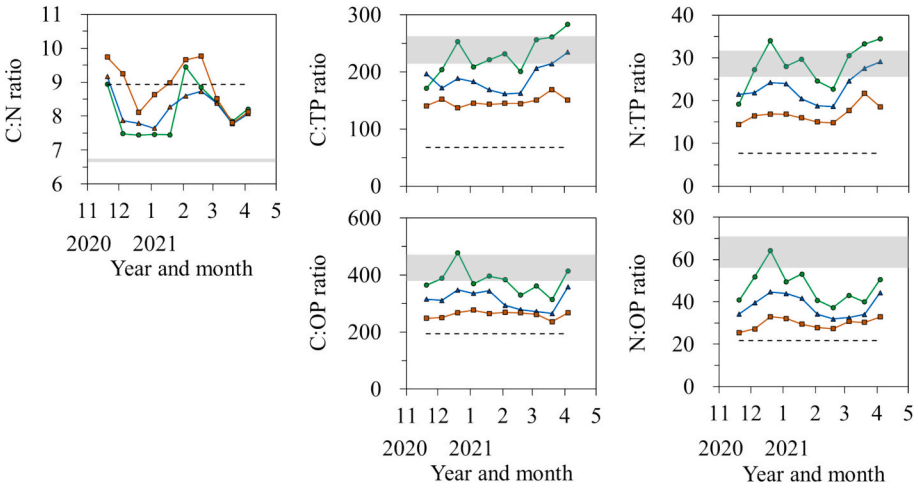

Fig. 5. Temporal variations in the C:N, N:TP, C:OP, and N:OP ratios (mol mol^{-1}) of sinking particles at water depths of 500 m (●), 1000 m (▲), and 2250 m (■). For each ratio, the dashed horizontal line represents the mean value in the surface sediment, and the gray shaded area is bounded by the mean values of suspended particles in the surface waters in May and November.

30 at 500, 1000, and 2250 m, respectively; and 22 in the surface sediment (Fig. S2). A similar decreasing trend was observed for the C:TP and N:TP ratios, with values of 238, 229, 189, 148, and 68 for C:TP and 36, 28, 23, 17, and 7.6 for N:TP for the suspended particles in surface waters, at 500, 1000, and 2250 m, and surface sediment, respectively (Fig. S2). Notably, the C:TP and N:TP ratios in the sediment were significantly lower than those in the upper water column, and also lower than the Redfield ratios (Fig. 5).

Regarding the seasonal differences in C:N:TP ratios in the suspended particles, the mean C:N ratios were similar in November (6.7) and May (6.8) (Fig. 5, Table S2). In contrast, the mean C:TP and N:TP ratios were higher in November (262 and 40) than in May (213 and 32, respectively). Similarly, the mean C:OP and N:OP ratios were higher in November (471 and 71, respectively) than in May (377 and 56, respectively) (Fig. 5).

The C:N ratios in the sinking particles at all three depths varied within a similar range (7.4–9.8) (Fig. 5; Table S1). In contrast, the C:TP and N:TP ratios exhibited greater variability at 500 m (171–283 and 19–34, respectively) than at the other depths, whereas the values at 2250 m showed much smaller variations (137–169 and 14–22, respectively). Similar variation patterns were observed when OP was considered instead of TP (Fig. 5). The elemental ratios exhibited distinct temporal trends (Fig. 5, Table S1). The C:N ratios at 500 m decreased from November (8.9) to late December (7.4), remained constant until January, increased in February (9.5), and then decreased until late March (7.8) (Fig. 5). The C:N ratios at 1000 m decreased from November (9.2) to January (7.6), increased until February (8.7), and then decreased until late March (7.8). The C:N ratios at 2250 m decreased from November (9.7) to late December (8.1), increased until late February (9.8), and then decreased until late March (7.8). The C:TP and N:TP ratios at 500 m generally increased from November (171 and 19.1, respectively) to early April (283 and 34, respectively), reaching maxima in early April (Fig. 5). When OP was used instead of TP at 500 and 1000 m, the increase in the ratios from February to April was less pronounced (Fig. 5).

3.5. Contents and fluxes of lithogenic material, opal, and $CaCO_3$ in the sinking particles

The lithogenic content was similar at 500 and 1000 m, but significantly higher at 2250 m (Fig. 6; Table 1). The opal content was higher at 500 m than at greater water depths. Opal was a dominant component at 500 and 1000 m, while the lithogenic content was dominant at 2250 m (Table S1). $CaCO_3$ had the smallest contribution of all the major components in the samples. At all depths, the sum of lithogenic material, opal, $CaCO_3$, and POM was 100 % ± 3 % of the total mass. The summed value for the sample collected at 1000 m in January was only 51 % of the total mass (indicated by the parentheses in Fig. 6), which we suspect was a weighing error during analysis, although we were unable to confirm this.

Temporally, the lithogenic content at 500 m was relatively high in November (36.4 wt%) and December (39.0 wt%), and then gradually decreased until April (11.1 wt%), reaching about one-third of the November value (Fig. 6). In contrast, the opal content gradually increased from November (33.6 wt%) to April (65.9 wt%) (Fig. 6). This inverse relationship between lithogenic and opal contents was also observed at 1000 and 2250 m (Fig. 6). At 500 and 1000 m, the $CaCO_3$ content reached a maximum in January, decreased to a minimum in late March, and then increased again in April. At 2250 m, the $CaCO_3$ content showed much smaller temporal variations (Fig. 6).

The average lithogenic fluxes were 107, 121, and 234 mg m^{-2} d^{-1} at 500, 1000, and 2250 m, respectively (Table 1). The lithogenic flux at 2250 m was the highest throughout the period, and nearly twice that at 500 m (Fig. 6). The average opal fluxes were 190, 205, and 222 mg m^{-2} d^{-1} at 500, 1000, and 2250 m, respectively; the 2250 m flux was ~20 % higher than that at 500 m, but comparable to that at 1000 m (Table 1). In contrast, average $CaCO_3$ fluxes were similar at all depths (35 ± 21 mg m^{-2} d^{-1}) (Table 1).

The lithogenic flux peaked in November at all water depths (Fig. 6). The lithogenic flux at 500 and 1000 m decreased until late December, and then remained constant. At 2250 m, an additional peak occurred in

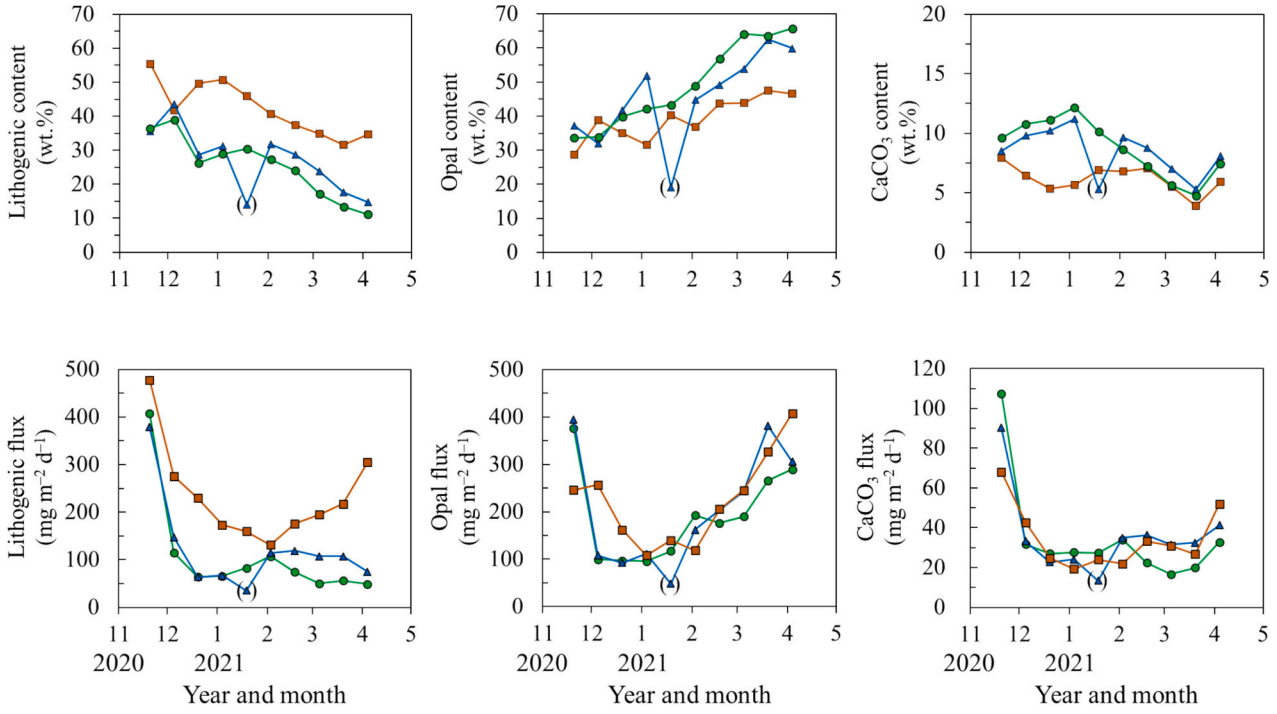

Fig. 6. Temporal variations in the contents and fluxes of lithogenic material, opal, and $CaCO_3$ at water depths of 500 m (●), 1000 m (▲), and 2250 m (■). An anomalous sample, for which the sum of lithogenic material, opal, and $CaCO_3$, and particulate organic matter (POM) accounted for only 51 % of the total mass, is indicated by parentheses.

April, reaching ~60 % of the November maximum, which was not observed at the upper two depths. The opal flux peaked in November at 500 and 1000 m and then increased steadily from January to April, reaching ~80 % of the flux in November. The $CaCO_3$ flux was highest in November at all water depths, remained stable thereafter, and increased slightly in April.

4. Discussion

4.1. Particulate P speciation and cycling

The mean C:N:TP ratios (238:36:1) of the surface suspended particles differed from the mean C:N:TP stoichiometry (107:11:1; $n = 6$) reported by Chen et al. (1996) in the southwestern East Sea, demonstrating considerable variability in the stoichiometry within the same region. Chen et al. (1996) reported that the C:TP ratios varied over a wide range from 61 to 132, and N:TP ratios ranged from 6 to 14. In our study, the C:TP and N:TP ratios were 107–328, and from 17 to 51, respectively (Table S2). As such, the C:N:P stoichiometry appears to vary considerably. The temporal and spatial variations in C:N:P ratios could be caused by various factors, such as the presence of partially degraded organic matter, preferential degradation of P (Paytan et al., 2003), nutrient availability (Galbraith and Martiny, 2015), and nature of the planktonic community (Karl et al., 2001; Liefer et al., 2024). Unfortunately, we do not have the data needed to identify the major factor responsible for the observed variability.

Notably, the proportions of IP relative to TP were comparable to the proportions of OP relative to TP in the suspended particles (Table S2). Non-biogenic IP can be supplied mainly by river input or atmospheric deposition. There is no major river draining into the study region to supply terrigenous particles. Also, given that the input of terrigenous Al from atmospheric deposition is minor in this region (Seo et al., 2023), we propose that most of the IP was biologically derived, such as polyphosphate (Diaz et al., 2008, 2012). Because the IP fraction defined in our study may also contain loosely adsorbed P, this methodological aspect may have contributed to high IP content in these samples (Eixler et al., 2005).

In surface sediments, a large fraction of TP was present as IP (Fig. 4). The TP contents did not decrease from that of the sinking particles at 2250 m, apparently because an increase in the IP compensated for the decrease in OP. As a result, the C:TP and N:TP ratios were low (68 and 7.6, respectively). The increase in the IP contents in the surface sediments, as compared with the sinking particles (Fig. 4), may result from the transformation of OP to IP during the degradation of organic matter in the sediment. For example, the "sink–switch" process refers to the transformation of P species during organic matter degradation and Fe oxide reduction in sediment, whereby particulate P is released as dissolved inorganic phosphate and subsequently precipitates either as structurally stable carbonate fluorapatite or is adsorbed onto Fe oxides in surface sediment (Lehtoranta et al., 2009; Paytan and McLaughlin, 2007). In the present study, the NAIP fraction accounted for ~80 % of the IP in the surface sediment (Table 1), indicating that most of the IP was in a mineral-bound form.

In sinking particles, decreasing trends in the C:TP and N:TP ratios, as well as in the C:OP and N:OP ratios, were observed from 500 to 2250 m (Fig. 5). These decreases are attributed primarily to reductions in POC and N contents rather than increases in P contents. The POC and N contents decreased by at least ~20 % across the depth intervals, whereas the TP and OP contents remained relatively stable (Table 1). Gerace et al. (2023) also reported a decreasing trend in the C:P ratios of suspended particles with increasing water depth in the upper 500 m layer in the Sargasso Sea. They attributed a decrease in the C:P ratios to more rapid degradation of carbohydrates as compared with lipids as the dissolved oxygen concentrations decrease. To properly understand the C:N:P stoichiometry along the biological pump, it is necessary to consider changes in both contents and fluxes with increasing water depth. In our study, the fluxes of POC, PN, and P species were higher at 2250 m. Sediment resuspension is prevalent in the UB (Kim et al., 2017; Kim et al., 2020), and the sinking particles also contained a high fraction of resuspended material. This complicates the interpretation of depth-dependent trends in particle decomposition and necessitates quantification of the contribution of resuspension to the sinking particles.

An interesting aspect of the UB in terms of trace metal cycling is that surface sediment contains very high amounts of Fe and Mn (~3.2 wt% Fe, ~1.1 wt% Mn, and ~ 4.8 wt% Al; Cha et al., 2007). These metals are known to retain IP via adsorption (Ruban et al., 1999). If such sediment, characterized by a high IP content (mainly NAIP), is resuspended and supplied to the water column, it will affect the particulate C:N:P stoichiometry. In our study, both the lithogenic fluxes and contents were higher at 2250 m than at 500 and 1000 m, and the NAIP accounted for >70 % of the IP in the sinking particles at all depths (Table 1). These results suggest that resuspension of IP-rich surface sediment contributed to the elevated IP contents and fluxes in the sinking particles. The high dissolved oxygen concentrations in the East Sea could have suppressed the reductive dissolution of metal oxides that would otherwise release IP under anoxic conditions (Benitez-Nelson et al., 2007).

At the study site, the Al and IP fluxes were strongly correlated (when the first sampling period at 500 m water depth is excluded: $R^2 = 0.95$ and $p < 0.001$; when it is included: $R^2 = 0.73$ and $p < 0.001$), supporting that IP was indeed supplied by resuspended lithogenic material (Fig. 7). The y-intercept of the regression line was very low (0.8 μmol m^{-2} d^{-1}), suggesting that IP unassociated with lithogenic material (i.e., biogenic IP sinking from the surface) was minimal. In the first sampling period at 500 m water depth in November 2020, the IP flux was much higher than during the other sampling periods (Fig. 7), demonstrating that IP derived from primary production can be transported rapidly to the deep sea when the biogenic particle flux is high (Armstrong et al., 2001).

4.2. Reconstruction of primary-production-driven fluxes of C, N, and P, and their stoichiometry in the Ulleung Basin

Based on the strong relationship between the lithogenic and IP fluxes, we divided the observed fluxes into the biogenic and sediment-resuspension-derived fluxes (Fig. 8; Methods section). We assumed that the elemental molar ratios in the surface sediment remained unchanged after resuspension. The resuspension-derived fluxes of POC, PN, OP, and IP were highest at 2250 m as expected (Fig. 8; Table S3). The resuspension-derived IP flux was nearly identical to the observed IP flux at 1000 and 2250 m (Fig. S3). The relative contributions of resuspension-derived POC, PN, and OP were smaller than that of IP, accounting for up to ~30 % at 2250 m, indicating that the IP fluxes were the most strongly affected by sediment resuspension.

We estimated the biogenic fluxes from the overlying water column

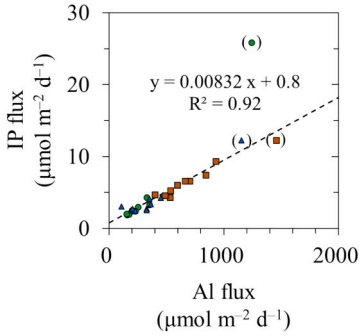

Fig. 7. Plot of the IP flux versus the Al flux at water depths of 500 m (●), 1000 m (▲), and 2250 m (■). The linear regression was obtained after excluding the samples from the first sampling period in November at all depths (indicated by parentheses).

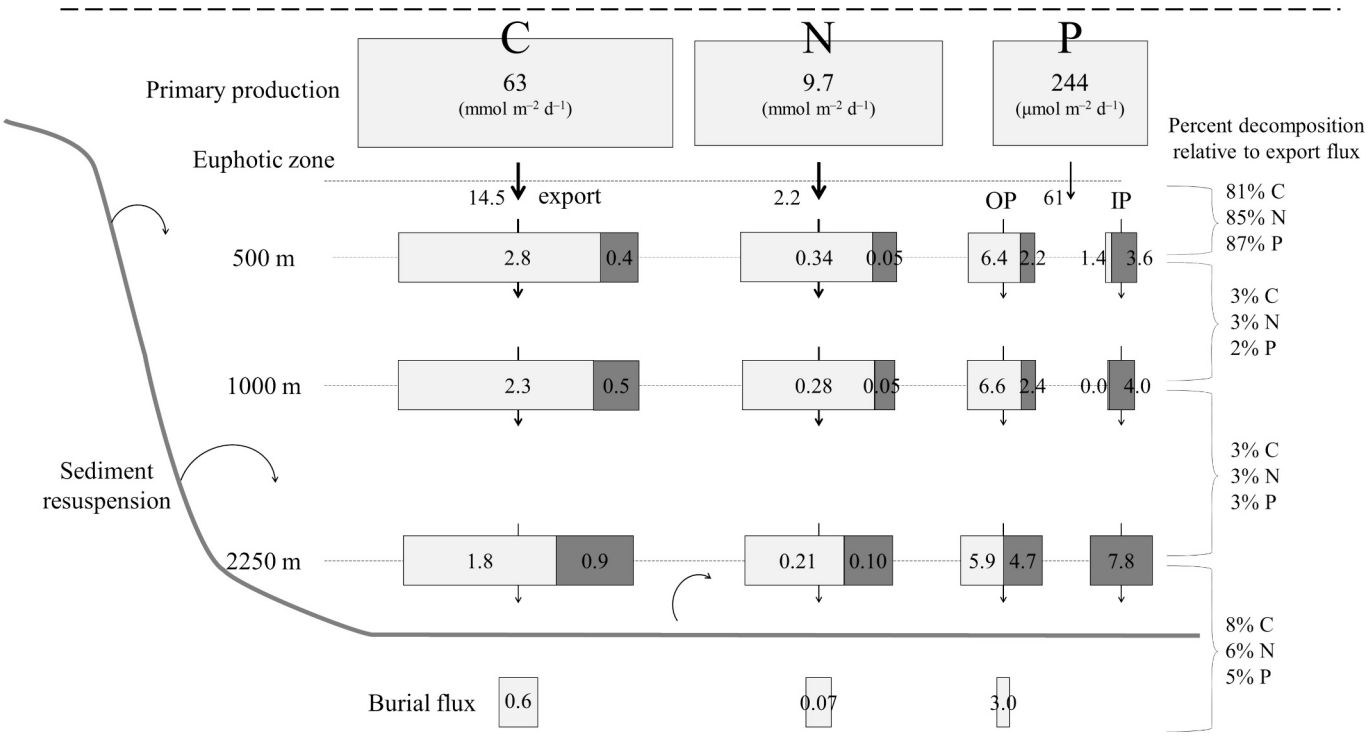

Fig. 8. Fluxes of C, N, and P at the sediment trap mooring site. The primary-production-derived vertical fluxes (light gray boxes) and resuspension-derived fluxes (dark gray boxes) are shown separately. Note that the sizes of the boxes are not to scale. Units are mmol m^{-2} d^{-1} for C and N, and μmol m^{-2} d^{-1} for P. Percentages of decomposition relative to the export flux at each depth interval are shown at far right.

by subtracting the resuspension-derived component from each elemental flux (Fig. 8). Because direct measurements of primary production, export production, and burial fluxes were not conducted at the study site, literature values were used. For the primary production, the average values of 273 g C m^{-2} yr^{-1} (Kwak et al., 2013) and 280 g C m^{-2} yr^{-1} (Joo et al., 2014) were used. An export ratio (e-ratio) of 0.23 was adopted from a satellite-data-based modeling study (Joo et al., 2018), and from a modeling study using ^{3}H-^{3}He dating and apparent oxygen utilization (Hahm and Kim, 2008). The burial flux was estimated from the ^{210}Pb-based sediment accumulation rate (2.56 g C m^{-2} yr^{-1}; Lee et al., 2010), and the C, N, and OP contents of the surface sediment.

By considering only the primary-production-derived fluxes (Fig. 8; Table S3), we estimated the degree to which the fluxes decreased relative to export production at each depth interval. Biogenic C, N, and P decomposed by 81 %–87 % between export and reaching 500 m. Flux attenuation for P (87 %) and N (85 %) was slightly larger than for C. Subsequently, only an additional 2 %–3 % decomposed in the 500–1000 m and 1000–2250 m depth intervals. Further substantial degradation occurred after deposition on the seafloor. Only 5 % of the C, 3 % of the N, and 3 % of the P were ultimately incorporated into the burial flux. These results demonstrate that most organic matter degradation occurs in the upper 500 m of the water column (Buesseler and Boyd, 2009; Steinberg et al., 2008). The greater relative loss of P as compared with C and N within this depth interval implies that P is more susceptible to degradation at the early stage of organic matter degradation (Paytan and McLaughlin, 2007; Tanioka et al., 2021; Xiang et al., 2023).

When considering the changes in the C:N:P stoichiometry, it is important to determine which P fraction (i.e., TP or OP) represents the biogenic material. For suspended particles in the surface waters, as discussed in Section 4.1, a considerable fraction of the IP was likely biologically derived. In contrast, the IP at 500 m was derived mainly from resuspended sediment. Taken together, these observations suggest that the IP in the surface layer is labile and rapidly decomposed (Faul et al., 2005). As such, the C:TP ratio appears to be more appropriate than the C:OP ratio as a measure of the biological stoichiometry in surface waters (<500 m water depths). In contrast, for sinking particles, because there is selective input to sinking particles of P relative to C and N derived from resuspended sediment, the inclusion of IP would lower the C:P and N:P ratios and bias the biological stoichiometry. We suggest that the C:OP provides a better measure of the biological stoichiometry for sinking particles in an environment where sediment resuspension is prevalent.

The mean C:N ratios of the biogenic particles, excluding resuspended sediment, were 6.7, 8.1, 8.1, 8.9, and 9.3 in surface suspended particles, sinking particles at water depths of 500, 1000, and 2250 m, and surface sediments, respectively (Fig. 9). The biogenic C:N ratios increased between the surface and 500 m water depth, and remained nearly constant below this depth. The mean biogenic C:P ratios were 238, 444, 359, 329, and 109, and the mean biogenic N:P ratios were 36, 56, 45, 37, and 12 at the depths corresponding to the C:N ratios. Both the C:P and N:P ratios increased between the surface waters and 500 m depth, subsequently decreased to 2250 m, and then decreased considerably in the surface sediment.

The elevated biogenic C:P and N:P ratios between the near-surface suspended particles and sinking particles at 500 m suggest there is preferential degradation of P in the upper water column (Fig. 9). Below 500 m, the decrease in the biogenic C:P and N:P ratios likely reflects the preferential degradation of C- and N-containing compounds. Together with the increasing C:N ratio, this interpretation is consistent with the preferential degradation of carbohydrates and amino acids (Gerace et al., 2023; Henderson et al., 2025). The decrease in biogenic C:P ratios between 1000 and 2250 m was smaller than that in the overlying upper water column, suggesting that preferential degradation of C relative to P was less pronounced in this depth interval. The C:P ratio decreased to

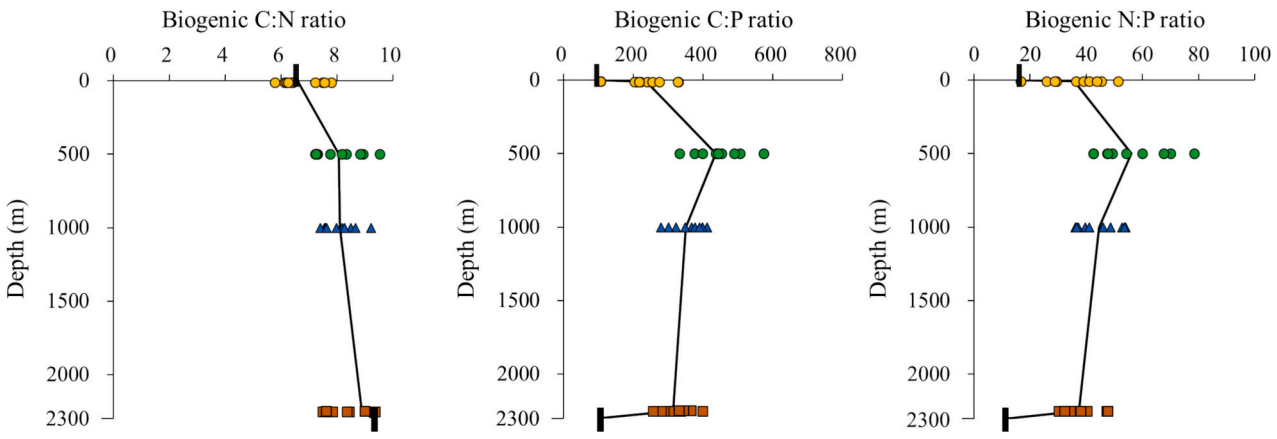

Fig. 9. Vertical profiles of the C:N, C:P, and N:P ratios (mol mol^{-1}) in the biogenic material, excluding the contribution from sediment resuspension. Colored symbols represent stoichiometric ratios for suspended (○) and sinking (●, ▲, and ■) particles at each depth. The vertical lines connect the mean ratios, starting from the primary production value assuming the Redfield ratio (106:16:1) and ending at the surface sediment value (109:12:1). This line is only a visual guide and does not indicate interpolation between the values.

approach the Redfield ratio while the C:N ratio increased further (Fig. 9), implying more degradation of C and N than P upon sedimentation.

5. Conclusions and implications

This paper has presented the first measurements of P species in the UB, including surface particles, sinking particles, and surface sediments. Phosphorus in the sinking particles consists of ~60 % OP and ~ 30 % IP. More than 70 % of the IP was NAIP. The POC and PN contents exhibit similar temporal and depth-related variations, while the OP contents exhibit smaller variations. In contrast to the OP, the IP contents have greater temporal changes and increase with water depth, peaking at 2250 m. The IP fluxes have a strong correlation with the Al flux and increase with depth, because the effect of sediment resuspension is greater towards the seafloor. The Al:IP ratio of the sinking particles is similar to that of the surface sediment. This suggests that IP is tightly bound to lithogenic material and is likely supplied to the water column by sediment resuspension. Therefore, IP should be excluded when evaluating the biological C:N:P stoichiometry in sinking particles, particularly in marginal seas where sediment resuspension is prevalent. If P speciation is not considered, the biogenic P content might be overestimated. In contrast, particulate IP in the surface waters is labile and rapidly decomposed before reaching 500 m water depth. Therefore, TP appears to be an appropriate parameter for evaluating biological C:N:P stoichiometry in the surface layer. The preferential remineralization of labile OP and IP appears to occur mostly between the surface and 500 m water depth, leading to elevated C:N, C:P, and N:P ratios at 500 m depth. Below 1000 m water depth, C:N ratios are either slightly higher or remain stable, whereas C:P and N:P ratios decrease progressively with depth, likely due to selective remineralization in the order N > C > P. Opal appeared to be associated with more efficient transport of biogenic OP to the deep sea. However, due to the lack of relevant measurements, the details of this remain uncertain. Nevertheless, without considering P speciation or correcting for the resuspension-derived fraction, correlations between the C:P ratio and opal content are absent or weak, suggesting that these approaches may provide important insights into the biogeochemical drivers of C:N:P stoichiometry in sinking particles. The C:P and N:P ratios still exhibited large temporal variability when the influence of resuspension-derived C, N, and P was excluded. Therefore, the C:N:P ratios measured at a single time point may not fully represent the overall characteristics of the study area, highlighting the importance of time-series data for evaluating the reliable C:N:P stoichiometry.

CRediT authorship contribution statement

Chihyun Oh: Writing – original draft, Visualization, Validation, Investigation, Formal analysis, Conceptualization. **Taehee Na:** Writing – review & editing, Project administration, Formal analysis. **Jeomshik Hwang:** Writing – review & editing, Supervision, Project administration, Funding acquisition, Conceptualization.

Declaration of competing interest

The authors declare that they have no known competing financial interests or personal relationships that could have appeared to influence the study reported in this paper.

Acknowledgements

This research was supported by the “Mid-Career Bridging Program” funded by Seoul National University and the “The Carbon Cycle Between Oceans, Land, and Atmosphere (RS-2022-NR068501)” project grant from the National Research Foundation that was funded by the Ministry of Science and ICT, Korea. This research was also supported by the Korea Institute of Marine Science and Technology Promotion (KIMST), which is funded by the Ministry of Oceans and Fisheries, Korea (Grant 20220541; Changes in the Physical and Biogeochemical Environment in the Tsushima Warm Current System of Korean Waters).

Appendix A. Supplementary data

Supplementary data to this article can be found online at https://doi.org/10.1016/j.marchem.2025.104601.

Data availability

Data will be made available on request.

References

Armstrong, R.A., Lee, C., Hedges, J.I., Honjo, S., Wakeham, S.G., 2001. A new, mechanistic model for organic carbon fluxes in the ocean based on the quantitative association of POC with ballast minerals. Deep-Sea Res. II Top. Stud. Oceanogr. 49 (1–3), 219–236. https://doi.org/10.1016/S0967-0645(01)00101-1.

Arrigo, K.R., Robinson, D.H., Worthen, D.L., Dunbar, R.B., DiTullio, G.R., VanWoert, M., Lizotte, M.P., 1999. Phytoplankton community structure and the drawdown of nutrients and CO2 in the Southern Ocean. Science 283 (5400), 365–367. https://doi.org/10.1126/science.283.5400.365.

Behrenfeld, M.J., Falkowski, P.G., 1997. Photosynthetic rates derived from satellite-based chlorophyll concentration. Limnol. Oceanogr. 42 (1), 1–20. https://doi.org/10.4319/lo.1997.42.1.0001.

Benitez-Nelson, C.R., Madden, L.P.N., Styles, R.M., Thunell, R.C., Astor, Y., 2007. Inorganic and organic sinking particulate phosphorus fluxes across the oxic/anoxic water column of Cariaco Basin, Venezuela. Mar. Chem. 105 (1–2), 90–100. https://doi.org/10.1016/j.marchem.2007.01.007.

Buesseler, K.O., Boyd, P.W., 2009. Shedding light on processes that control particle export and flux attenuation in the twilight zone of the open ocean. Limnol. Oceanogr. 54 (4), 1210–1232. https://doi.org/10.4319/lo.2009.54.4.1210.

Cha, H.-J., Choi, M.S., Lee, C.-B., Shin, D.-H., 2007. Geochemistry of surface sediments in the southwestern East/Japan Sea. J. Asian Earth Sci. 29 (5–6), 685–697. https://doi.org/10.1016/j.jseaes.2006.04.009.

Chen, C.-T.A., Lin, C.-M., Huang, B.-T., Chang, L.-F., 1996. Stoichiometry of carbon, hydrogen, nitrogen, sulfur and oxygen in the particulate matter of the western North Pacific marginal seas. Mar. Chem. 54 (1–2), 179–190. https://doi.org/10.1016/0304-4203(96)00021-7.

Diaz, J., Ingall, E., Benitez-Nelson, C., Paterson, D., De Jonge, M.D., McNulty, I., Brandes, J.A., 2008. Marine polyphosphate: a key player in geologic phosphorus sequestration. Science 320 (5876), 652–655. https://doi.org/10.1126/science.1151751.

Diaz, J.M., Ingall, E.D., Snow, S.D., Benitez-Nelson, C.R., Taillefert, M., Brandes, J.A., 2012. Potential role of inorganic polyphosphate in the cycling of phosphorus within the hypoxic water column of Effingham inlet, British Columbia. Glob. Biogeochem. Cycles 26 (2). https://doi.org/10.1029/2011GB004226.

Eixler, S., Selig, U., Karsten, U., 2005. Extraction and detection methods for polyphosphate storage in autotrophic planktonic organisms. Hydrobiologia 533, 135–143. https://doi.org/10.1007/s10750-004-2406-9.

Faul, K.L., Paytan, A., Delaney, M.L., 2005. Phosphorus distribution in sinking oceanic particulate matter. Mar. Chem. 97 (3–4), 307–333. https://doi.org/10.1016/j.marchem.2005.04.002.

Galbraith, E.D., Martiny, A.C., 2015. A simple nutrient-dependence mechanism for predicting the stoichiometry of marine ecosystems. Proc. Natl. Acad. Sci. 112 (27), 8199–8204. https://doi.org/10.1073/pnas.1423917112.

Garcia, N.S., Sexton, J., Riggins, T., Brown, J., Lomas, M.W., Martiny, A.C., 2018. High variability in cellular stoichiometry of carbon, nitrogen, and phosphorus within classes of marine eukaryotic phytoplankton under sufficient nutrient conditions. Front. Microbiol. 9, 543. https://doi.org/10.3389/fmicb.2018.00543.

Gerace, S.D., Fagan, A.J., Primeau, F.W., Moreno, A.R., Lethaby, P., Johnson, R.J., Martiny, A.C., 2023. Depth variance of organic matter respiration stoichiometry in the subtropical North Atlantic and the implications for the global oxygen cycle. Glob. Biogeochem. Cycles 37 (12), e2023GB007814. https://doi.org/10.1029/2023GB007814.

Hahm, D., Kim, K.-R., 2008. Observation of bottom water renewal and export production in the Japan Basin, East Sea using tritium and helium isotopes. Ocean Sci. J. 43, 39–48. https://doi.org/10.1007/BF03022430.

Henderson, L.C., English, C.J., Jeng, D.L., Popendorf, K.J., Carlson, C.A., Close, H.G., 2025. Carbohydrate content controls vertical variations in carbon to nitrogen ratios of organic particles within the euphotic zone in the Northwest Sargasso Sea. Commun. Earth Environ. 6 (1), 547. https://doi.org/10.1038/s43247-025-02524-6.

Honjo, S., Dymond, J., Collier, R., Manganini, S.J., 1995. Export production of particles to the interior of the equatorial Pacific Ocean during the 1992 EqPac experiment. Deep-Sea Res. II Top. Stud. Oceanogr. 42 (2), 831–870. https://doi.org/10.1016/0967-0645(95)00034-N.

Joo, H., Park, J.W., Son, S., Noh, J.H., Jeong, J.Y., Kwak, J.H., Saux-Picart, S., Choi, J.H., Kang, C.K., Lee, S.H., 2014. Long-term annual primary production in the Ulleung Basin as a biological hot spot in the East/Japan Sea. J. Geophys. Res. Oceans 119 (5), 3002–3011. https://doi.org/10.1002/2014jc009862.

Joo, H., Lee, D., Son, S.H., Lee, S.H., 2018. Annual new production of phytoplankton estimated from MODIS-derived nitrate concentration in the East/Japan Sea. Remote Sens. 10 (5), 806. https://doi.org/10.3390/rs10050806.

Karl, D.M., Björkman, K.M., Dore, J.E., Fujieki, L., Hebel, D.V., Houlihan, T., Letelier, R. M., Tupas, L.M., 2001. Ecological nitrogen-to-phosphorus stoichiometry at station ALOHA. Deep-Sea Res. II Top. Stud. Oceanogr. 48 (8–9), 1529–1566. https://doi.org/10.1016/S0967-0645(00)00152-1.

Kim, K.-R., Kim, K., 1996. What is happening in the East Sea (Japan Sea)?: recent chemical observations during CREAMS 93-96. J. Korean Soc. Oceanogr. 31 (4), 164–172.

Kim, M., Hwang, J., Rho, T., Lee, T., Kang, D.-J., Chang, K.-I., Noh, S., Joo, H., Kwak, J. H., Kang, C.-K., 2017. Biogeochemical properties of sinking particles in the southwestern part of the East Sea (Japan Sea). J. Mar. Syst. 167, 33–42. https://doi.org/10.1016/j.jmarsys.2016.11.001.

Kim, M., Kim, Y.-I., Hwang, J., Choi, K.Y., Kim, C.J., Ryu, Y., Park, J.-E., Park, K., Park, J.-H., Nam, S., 2020. Influence of sediment resuspension on the biological pump of the southwestern East Sea (Japan Sea). Front. Earth Sci. 8, 538412. https://doi.org/10.3389/feart.2020.00144.

Koeve, W., Kähler, P., 2010. Balancing ocean nitrogen. Nat. Geosci. 3 (6), 383–384. https://doi.org/10.1038/ngeo884.

Kwak, J., Lee, S., Park, H., Choy, E., Jeong, H., Kim, K., Kang, C., 2013. Monthly measured primary and new productivities in the Ulleung Basin as a biological" hot spot" in the East/Japan Sea. Biogeosciences 10 (7), 4405–4417. https://doi.org/10.5194/bg-10-4405-2013.

Kwon, E.Y., Holzer, M., Timmermann, A., Primeau, F., 2022a. Estimating three-dimensional carbon-to-phosphorus stoichiometry of exported marine organic matter. Glob. Biogeochem. Cycles 36 (3), e2021GB007154. https://doi.org/10.1029/2021GB007154.

Kwon, E.Y., Sreeush, M., Timmermann, A., Karl, D.M., Church, M.J., Lee, S.-S., Yamaguchi, R., 2022b. Nutrient uptake plasticity in phytoplankton sustains future ocean net primary production. Sci. Adv. 8 (51), eadd2475. https://doi.org/10.1126/sciadv.add2475.

Lam, P.J., Doney, S.C., Bishop, J.K., 2011. The dynamic ocean biological pump: insights from a global compilation of particulate organic carbon, CaCO3, and opal concentration profiles from the mesopelagic. Glob. Biogeochem. Cycles 25 (3). https://doi.org/10.1029/2010GB003868.

Laws, E.A., Bannister, T., 1980. Nutrient-and light-limited growth of *Thalassiosira fluviatilis* in continuous culture, with implications for phytoplankton growth in the ocean 1. Limnol. Oceanogr. 25 (3), 457–473. https://doi.org/10.4319/lo.1980.25.3.0457.

Lee, T.-H., Kim, D.-S., Khim, B.-K., Choi, D.-L., 2010. Organic carbon cycling in Ulleung basin sediments, East Sea. Ocean Polar Res. 32 (2), 145–156. https://doi.org/10.4217/OPR.2010.32.2.145.

Lee, J.S., Han, J.H., An, S.U., Kim, S.H., Lim, D., Kim, D., Kang, D.J., Park, Y.G., 2019. Sedimentary organic carbon budget across the slope to the basin in the southwestern Ulleung (Tsushima) basin of the east (Japan) sea. J. Geophys. Res. Biogeosci. 124 (9), 2804–2822. https://doi.org/10.1029/2019jg005138.

Lehtoranta, J., Ekholm, P., Pitkänen, H., 2009. Coastal eutrophication thresholds: a matter of sediment microbial processes. AMBIO: a journal of the human. Environment 38 (6), 303–308. https://doi.org/10.1579/09-a-656.1.

Liefer, J.D., White, A.E., Finkel, Z.V., Irwin, A.J., Dugenne, M., Inomura, K., Ribalet, F., Armbrust, E.V., Karl, D.M., Fyfe, M.H., 2024. Latitudinal patterns in ocean C: N: P reflect phytoplankton acclimation and macromolecular composition. Proc. Natl. Acad. Sci. 121 (46), e2404460121. https://doi.org/10.1073/pnas.2404460121.

Lomas, M.W., Bates, N.R., Johnson, R.J., Steinberg, D.K., Tanioka, T., 2022. Adaptive carbon export response to warming in the Sargasso Sea. Nat. Commun. 13 (1), 1211. https://doi.org/10.1038/s41467-022-28842-3.

Lyons, G., Benitez-Nelson, C.R., Thunell, R.C., 2011. Phosphorus composition of sinking particles in the Guaymas Basin, Gulf of California. Limnol. Oceanogr. 56 (3), 1093–1105. https://doi.org/10.4319/lo.2011.56.3.1093.

Martiny, A.C., Pham, C.T., Primeau, F.W., Vrugt, J.A., Moore, J.K., Levin, S.A., Lomas, M. W., 2013. Strong latitudinal patterns in the elemental ratios of marine plankton and organic matter. Nat. Geosci. 6 (4), 279–283. https://doi.org/10.1038/ngeo1757.

Martiny, A.C., Vrugt, J.A., Lomas, M.W., 2014. Concentrations and ratios of particulate organic carbon, nitrogen, and phosphorus in the global ocean. Sci. Data 1 (1), 1–7. https://doi.org/10.1038/sdata.2014.48.

Matsumoto, K., Tanioka, T., Rickaby, R., 2020. Linkages between dynamic phytoplankton C: N: P and the ocean carbon cycle under climate change. Oceanography 33 (2), 44–52. https://doi.org/10.5670/oceanog.2020.203.

Mills, M.M., Arrigo, K.R., 2010. Magnitude of oceanic nitrogen fixation influenced by the nutrient uptake ratio of phytoplankton. Nat. Geosci. 3 (6), 412–416. https://doi.org/10.1038/ngeo856.

Mortlock, R.A., Froelich, P.N., 1989. A simple method for the rapid determination of biogenic opal in pelagic marine sediments. Deep Sea Res. Part A 36 (9), 1415–1426. https://doi.org/10.1016/0198-0149(89)90092-7.

Murphy, J., Riley, J.P., 1962. A modified single solution method for the determination of phosphate in natural waters. Anal. Chim. Acta 27, 31–36. https://doi.org/10.1016/S0003-2670(00)88444-5.

Paytan, A., McLaughlin, K., 2007. The oceanic phosphorus cycle. Chem. Rev. 107 (2), 563–576. https://doi.org/10.1021/cr0503613.

Paytan, A., Cade-Menun, B.J., McLaughlin, K., Faul, K.L., 2003. Selective phosphorus regeneration of sinking marine particles: evidence from 31P-NMR. Mar. Chem. 82 (1–2), 55–70. https://doi.org/10.1016/S0304-4203(03)00052-5.

Redfield, A., Ketchum, B., Richards, F., 1963. The influence of organisms on the composition of seawater. Sea 2, 26–77.

Reynolds, R.W., Rayner, N.A., Smith, T.M., Stokes, D.C., Wang, W., 2002. An improved in situ and satellite SST analysis for climate. J. Clim. 15 (13), 1609–1625. https://doi.org/10.1175/1520-0442(2002)015<1609:AIISAS>2.0.CO;2.

Ruban, V., López-Sánchez, J., Pardo, P., Rauret, G., Muntau, H., Quevauviller, P., 1999. Selection and evaluation of sequential extraction procedures for the determination of phosphorus forms in lake sediment. J. Environ. Monit. 1 (1), 51–56. https://doi.org/10.1039/a807778i.

Ruban, V., López-Sánchez, J., Pardo, P., Rauret, G., Muntau, H., Quevauviller, P., 2001. Harmonized protocol and certified reference material for the determination of extractable contents of phosphorus in freshwater sediments–a synthesis of recent works. Fresenius J. Anal. Chem. 370, 224–228. https://doi.org/10.1007/s002160100753.

Rudnick, R.L., Gao, S., 2003. 3.01 - composition of the continental crust. In: Holland, H. D., Turekian, K.K. (Eds.), Treatise on Geochemistry. Pergamon, Oxford, pp. 1–64.

Ruttenberg, K.C., 1992. Development of a sequential extraction method for different forms of phosphorus in marine sediments. Limnol. Oceanogr. 37 (7), 1460–1482. https://doi.org/10.4319/lo.1992.37.7.1460.

Sakshaug, E., Holm-Hansen, O., 1977. Chemical composition of *Skeletonema costatum* (Grev.) Cleve and Pavlova (monochrysis) Lutheri (droop) green as a function of nitrate-, phosphate-, and iron-limited growth. J. Exp. Mar. Biol. Ecol. 29 (1), 1–34. https://doi.org/10.1016/0022-0981(77)90118-6.

Seo, J., Kim, G., Seo, H., Na, T., Noh, S., Hwang, J., 2023. Sources and behaviors of particulate organic carbon, iron, and manganese in the bottom nepheloid layer of the southwestern East Sea (Japan Sea). Mar. Chem. 257, 104323. https://doi.org/10.1016/j.marchem.2023.104323.

Steinberg, D.K., Van Mooy, B.A., Buesseler, K.O., Boyd, P.W., Kobari, T., Karl, D.M., 2008. Bacterial vs. zooplankton control of sinking particle flux in the ocean's twilight zone. Limnol. Oceanogr. 53 (4), 1327–1338. https://doi.org/10.4319/lo.2008.53.4.1327.

Tanioka, T., Matsumoto, K., 2020. A meta-analysis on environmental drivers of marine phytoplankton C: N: P. Biogeosciences 17 (11), 2939–2954. https://doi.org/10.5194/bg-17-2939-2020.

Tanioka, T., Matsumoto, K., Lomas, M.W., 2021. Drawdown of atmospheric pCO2 via variable particle flux stoichiometry in the ocean twilight zone. Geophys. Res. Lett. 48 (22), e2021GL094924. https://doi.org/10.1029/2021GL094924.

Taylor, S.R., McLennan, S.M., 1985. The Continental Crust: Its Composition and Evolution.

Teng, Y.-C., Primeau, F.W., Moore, J.K., Lomas, M.W., Martiny, A.C., 2014. Global-scale variations of the ratios of carbon to phosphorus in exported marine organic matter. Nat. Geosci. 7 (12), 895–898. https://doi.org/10.1038/Ngeo2303.

Williams, J., Jaquet, J., Thomas, R., 1976. Forms of phosphorus in the surficial sediments of Lake Erie. J. Fish. Res. Board Can. 33 (3), 413–429. https://doi.org/10.1139/f76-063.

Xiang, Y., Quay, P.D., Sonnerup, R.E., Fassbender, A.J., 2023. Subtropical gyre nutrient cycling in the Upper Ocean: insights from a nutrient-ratio budget method. Geophys. Res. Lett. 50 (13), e2023GL103213. https://doi.org/10.1029/2023GL103213.

Zhao, M., Mills, B.J., Poulton, S.W., Wan, B., Xiao, K.-Q., Guo, L., Guo, Z., 2024. Drivers of the global phosphorus cycle over geological time. Nat. Rev. Earth Environ. 5 (12), 873–889. https://doi.org/10.1038/s43017-024-00603-4.